Astron. Astrophys. 339, 561–574 (1998)

ASTRONOMY AND ASTROPHYSICS

CO in absorption and emission toward compact extragalactic radio continuum sources

H.S. Liszt[1] **and R. Lucas**[2]

[1] National Radio Astronomy Observatory, 520 Edgemont Road, Charlottesville, VA 22903-2475, USA
[2] Institut de Radioastronomie Millimétrique, 300 Rue de la Piscine, F-38406 Saint Martin d'Hères, France

Received 18 March 1998 / Accepted 31 August 1998

Abstract. We have observed galactic λ2.6mm and λ1.3mm CO absorption and emission along nine lines of sight toward compact extragalactic mm-wave continuum sources, using the IRAM Plateau de Bure Interferometer and NRAO 12m telescopes. In absorption we detected some two dozen kinematic components, and nearly every feature known from HCO^+ spectra (Lucas and Liszt, 1996) has a direct CO counterpart: a few CO lines are missing or very weak in emission even when $\tau(\mathrm{CO}) \gtrsim 0.5$. The column densities of CO and HCO^+ are well correlated, but not linearly related. The widths of the CO lines are typically 15% smaller than those of HCO^+ (on average 0.75 km s^{-1} $vs.$ 0.86 km s^{-1}).

We derive ^{12}CO column densities $0.1 \lesssim N(^{12}\mathrm{CO}) \lesssim 20 \times 10^{15}$ cm^{-2} which are in all cases very small compared to the column of carbon nuclei expected for 1 magnitude of visual extinction, even allowing for substantial depletion. The partial thermal pressure of H_2 is inferred to be $1000 \leq n(\mathrm{H_2})T_\mathrm{K} \leq 12,000$ cm^{-3} K, with a median p/k = 3.2×10^3 cm^{-3} K. Thus the clouds are likely warm ($T_\mathrm{K} \approx$ tens of K), somewhat diffuse ($n(\mathrm{H_2}) \approx 50 - 300$ cm^{-3}), with the majority of the gas-phase carbon in the form of C^+ and perhaps even with a substantial fraction of H I in the thinnest cases.

The isotope ratios in the CO usually differ strongly from the local interstellar ratio which we have separately measured in these clouds to be ^{12}C/^{13}C = 60 (Lucas and Liszt, 1998); we find $15 \leq \mathrm{N}(^{12}\mathrm{CO})/\mathrm{N}(^{13}\mathrm{CO}) \leq 54$, declining with increasing $N(^{12}\mathrm{CO})$. The ^{13}CO/C^{18}O ratio seen in emission or absorption is typically 25 (instead of 8) and C^{18}O is very difficult to detect in emission even when $T_\mathrm{R}^*(^{12}\mathrm{CO})/T_\mathrm{R}^*(^{13}\mathrm{CO}) < 10$. Apparently, the relative abundance of ^{13}CO is typically greatly enhanced, even at very low extinction, and never diminished by selective photodissociation. One effect of this enhancement is that lines of ^{12}CO are substantially less optically thick than might otherwise have been inferred. There is little evidence for a general selective depletion of C^{18}O.

Key words: ISM: abundances – ISM: clouds – ISM: molecules – ISM: structure – radio lines: interstellar

Send offprint requests to: R. Lucas

1. Introduction

The role of carbon monoxide as a tracer of molecular gas is greatly complicated by our ignorance of the conditions under which its emission features are formed. The lines of the most abundant isotope ^{12}CO are almost invariably opaque and the relative abundances of optically-thin species like ^{13}CO and C^{18}O are not fixed. The competing processes of fractionation (Watson et al., 1976) and selective photodissociation (Bally and Langer, 1982; Van Dishoeck and Black, 1988; Kopp et al., 1996) are important in all but the darkest regions. As additional complications, the excitation of the isotopes is not necessarily identical, and even ^{12}CO is not necessarily thermalized. It seems that no matter how many aspects of the emission measurements are considered, additional assumptions or information are always needed ($e.g.$ White, 1997). The final result of the process of investigating the excitation of CO has been to adopt a posture of studied ignorance in which, whenever possible, the amount of molecular gas is simply assumed to be proportional to the integrated intensity of the J=1-0 line of ^{12}CO.

Direct measurement of the optical depths of CO lines can provide the 'missing' additional information needed to determine the quantity of carbon monoxide. Indeed, measurement of the optical depths of enough lines in the CO rotational ladder will suffice to determine the CO column density without recourse to any emission measurements at all: one must simply observe up to transitions where the population of the lower level becomes insignificant.

Until recently (Marscher et al., 1991) such measurements were not possible, but the creation of mm-wave interferometers capable of resolving out foreground emission (Guilloteau et al., 1992) has made it possible to study many molecules in absorption in those relatively few directions where suitable background continuum sources are available (Lucas and Liszt, 1993, 1994, hereafter LL93 and LL94) Indeed, recent observations of common molecules like OH, HCO^+, CN, HCN, C_2H, H_2CO, $etc.$ have established the surprising result that abundances very like those seen in dark clouds already occur even when $A_\mathrm{V} \lesssim 1$ (Lucas and Liszt 1996, 1997, hereafter LL96

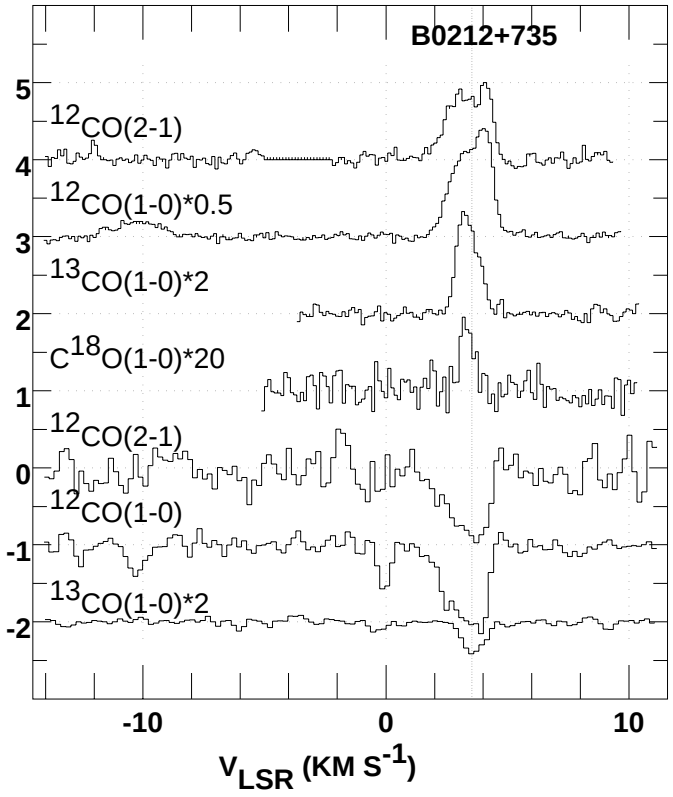

Fig. 1. CO absorption and emission profiles toward B0212+735, scaled in various ways as noted beneath the spectra.

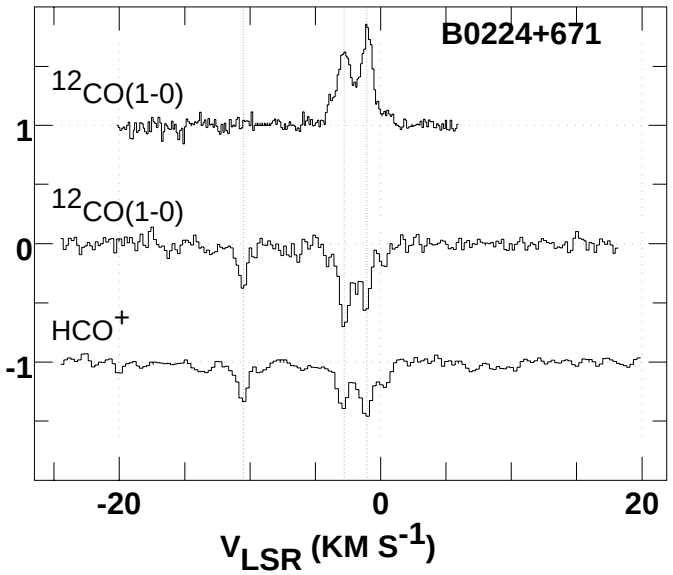

Fig. 2. As in Fig. 1, but for B0224+671. For comparison, the HCO^+ absorption spectrum is also shown.

and LL97; Hogerheijde et al. 1995; Liszt and Lucas 1994; Kobulnicky et al. 1995; Liszt and Lucas 1996).

The clouds occulting mm-wave continuum sources are diffuse rather than dark or even really translucent (LL96, LL97). Because of this, the column density of CO is in all cases very small compared to the amount of carbon in a gas column with

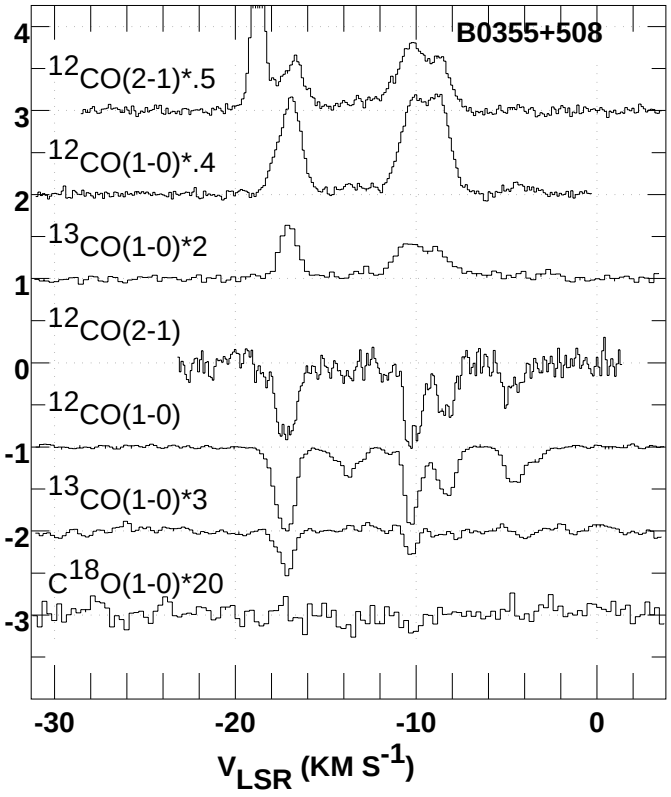

Fig. 3. As in Fig. 1, but for B0355+508 = NRAO150. The strong feature at -19 km s^{-1} in the J=2-1 spectrum at top is telluric.

1 magnitude of optical extinction, even allowing for depletion. These low column densities are actually somewhat fortuitous for the following reason. In the limit of pure radiative excitation by the cosmic microwave background ($T_{\rm ex} = T_{\rm cmb}$), it follows from the basic molecular constants that the integrated optical depth of the J=1-0 line of CO is 1.0 km s^{-1} when N(CO) = 1.0×10^{15} cm^{-2}. This is about half the CO column density in the archetypal diffuse gas seen toward ζ Oph (Kopp et al., 1996; Liszt, 1997), but less than 1% of the C^+ column density in that direction (Morton, 1975; Lambert et al., 1994). Given the availability of so much more carbon for making CO, it could easily have been the case that the low-lying CO lines from all chemically interesting clouds were hopelessly saturated. But the excitation and linewidth increase with cloud column density to such an extent that the beam-averaged, inferred, optical depth of the J=1-0 CO lines emitted from Orion KL, where N(CO) = 3×10^{19} cm^{-2}, is not any larger than seen here in those few clouds with N(CO) $\gtrsim 10^{16}$ cm^{-2}.

When clouds are studied in absorption against stars, the extinction and hydrogen column density are usually known; the nearness of the star bounds the distance of the absorbing gas, perhaps rendering the absorption spectrum somewhat simpler. By contrast, the material studied at radiofrequencies against extragalactic objects exists over longer sightlines through the entire galactic gas layer, usually at fairly low galactic latitudes (Liszt and Wilson, 1993; Liszt, 1994). This gas is somewhat harder to characterize, because of the overlap of multiple

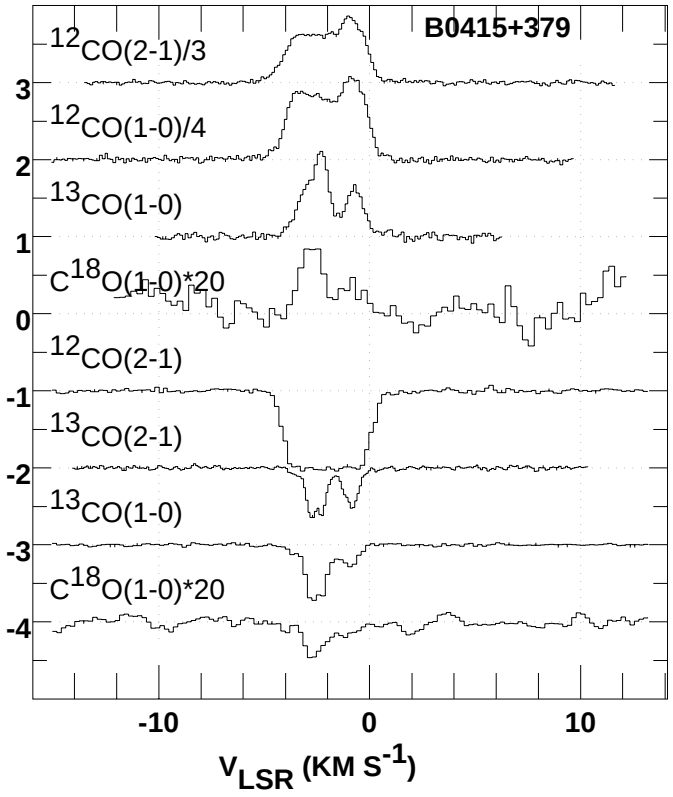

Fig. 4. As in Fig. 1, but for B0415+379 = 3C111.

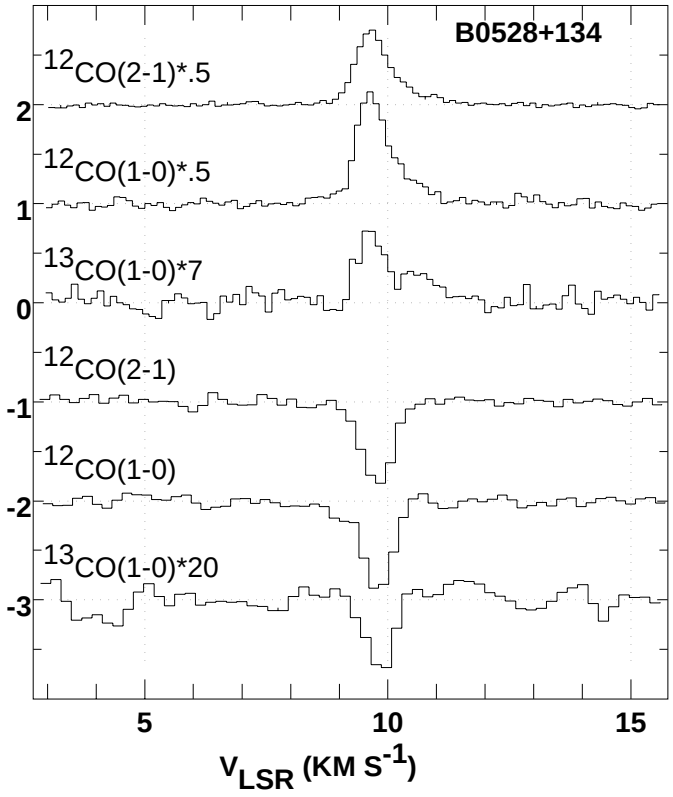

Fig. 5. As in Fig. 1, but for B0528+134.

kinematic components and the blending of ionized, atomic and molecular constituents. Even knowing the extinction toward a background source, which we do in only a small number of cases [1], is of little use when the arrangement of material along the line of sight is even moderately complex.

In this work, we have observed CO emission and absorption toward some of those objects toward which we have previously observed OH, HCO^+, and various other, rarer, high-dipole moment species in absorption. Observations of CO absorption are somewhat harder owing to (i) the increased optical depth and noise signal of the earth's atmosphere; (ii) the care needed to resolve out all foreground emission (which is much weaker when dealing with species having higher permanent dipole moments, as shown directly in LL96); (iii) the high signal/noise ratios needed to measure the optical depth precisely in even moderately opaque lines. Also, emission measurements are needed to estimate the excitation temperature when we have observed too few transitions in absorption. Nonetheless, the results are important because CO tells much about the character of the host gas, and because we learn how the CO 'turns on' under conditions where photodissociation is important, as at the outer edges of darker material.

In Sect. 2 we describe the new observations of CO emission and absorption which are presented here. In Sect. 3 we discuss the derivation of parameters from the observed lines, chiefly the column density and excitation temperature. In Sect. 4 we discuss general properties of the CO observations (linewidths, excitation temperatures, line brightness, relationship between emission and aborption, $etc.$) and the inferred physical parameters of the host gas (temperature, pressure) as derived from the CO lines. In Sect. 5 we discuss some relationships between molecular and isotopic species, emphasizing the importance of strong chemical fractionation at low extinction: earlier studies of emission across dark clouds had led to the conclusion that such effects were absent in diffuse and translucent gas. Sect. 6 is a summary.

Table 1. Background Source List and J=1-0 Rms

Source	Alias	l °	b °	$\sigma_{l/c}$ ^{13}CO	$\sigma_{l/c}$ ^{12}CO
B0212+735		128.93	11.96	0.037	0.085
B0224+671	4C67.05	132.12	6.23		0.045
B0355+508	NRAO150	150.38	−1.60	0.015	0.014
B0415+379	3C111	161.68	−8.82	0.011	
B0528+134		191.37	−11.01	0.005	0.043
B1730−130	NRAO530	12.03	10.81	0.006	0.011
B2013+370		74.87	1.22		0.039
B2200+420		92.13	−10.40	0.025	0.022
B2251+158	3C454.3	86.11	−38.18	0.004	0.009

[1] toward BL Lac, $A_V \approx 1$, from DuPuy et al. (1969); toward 3C111, $A_V < 1.3$ mag, see Ungerer et al. (1985)

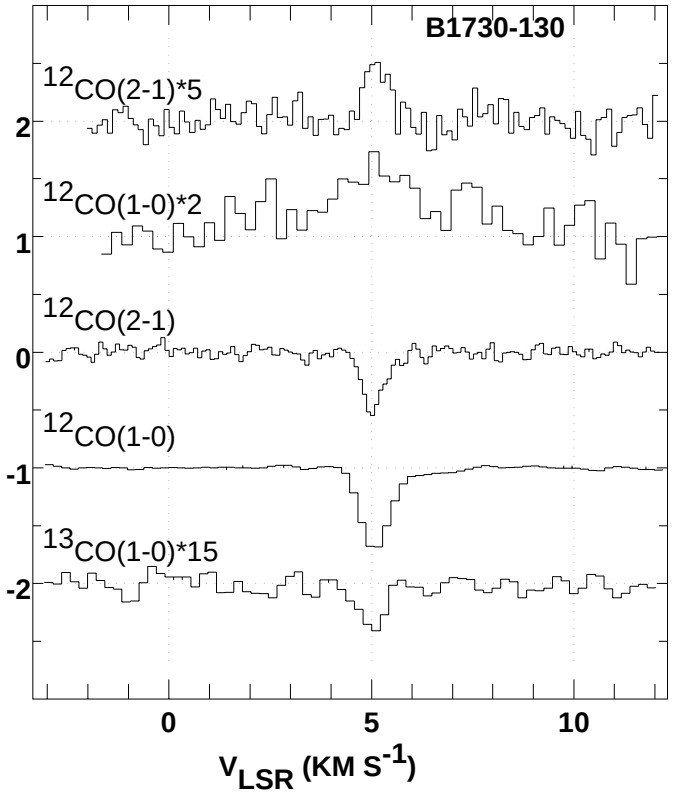

Fig. 6. As in Fig. 1, but for B1730-130 = NRAO530.

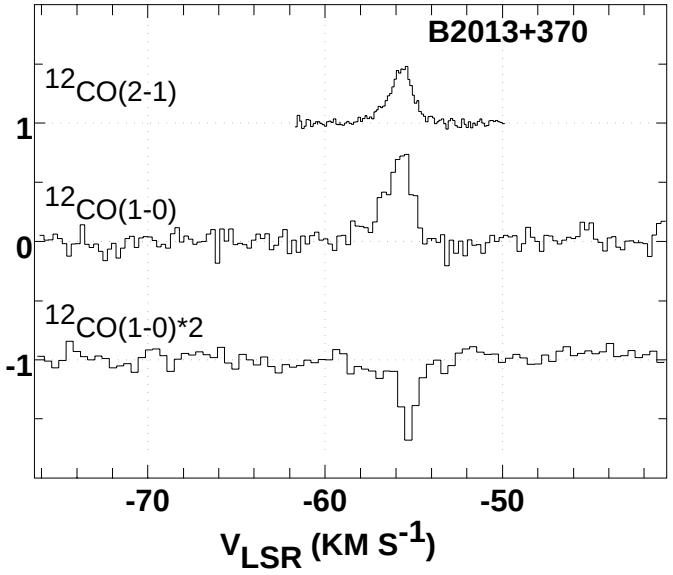

Fig. 7. As in Fig. 1, but for a portion of the spectrum toward B2013+370.

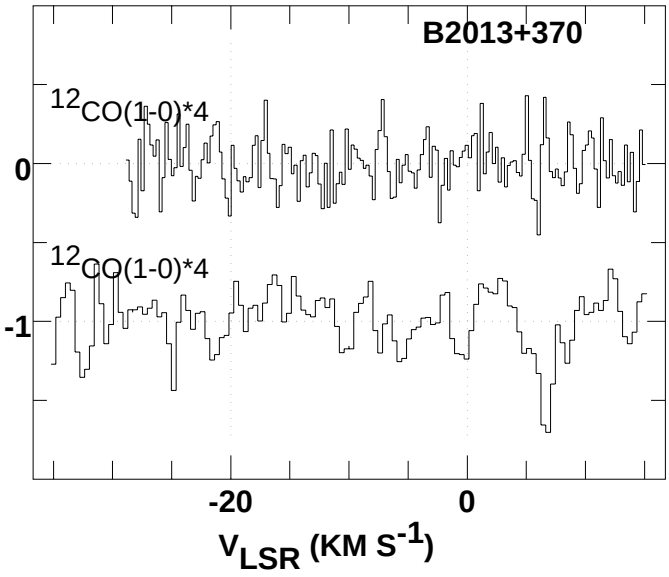

Fig. 8. As in Fig. 1, but for a portion of the spectrum toward B2013+370.

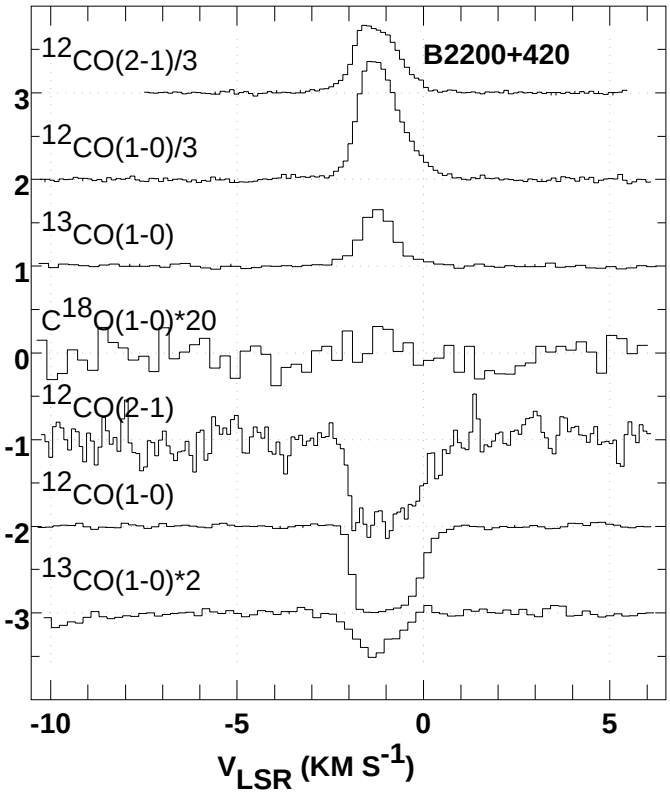

Fig. 9. As in Fig. 1, but for B2200+420 = BL Lac. The uppermost four spectra are of emission.

2. Our data

2.1. CO absorption line profiles

The CO absorption observations discussed here were taken at the Plateau de Bure Interferometer (Guilloteau et al., 1992) during the 1993-1996 observing seasons. The spectra have a channel spacing of 78 kHz and a resolution 140 kHz which for the J=1-0 transition correspond to 0.20 and 0.36 km s^{-1} for ^{12}CO, or 0.21 and 0.38 km s^{-1} for ^{13}CO and C^{18}O. The data have been treated in a manner generally similar to that discussed in LL96. In the case of CO, however, structure in the emission profiles may contaminate the absorption profiles. We have found that in

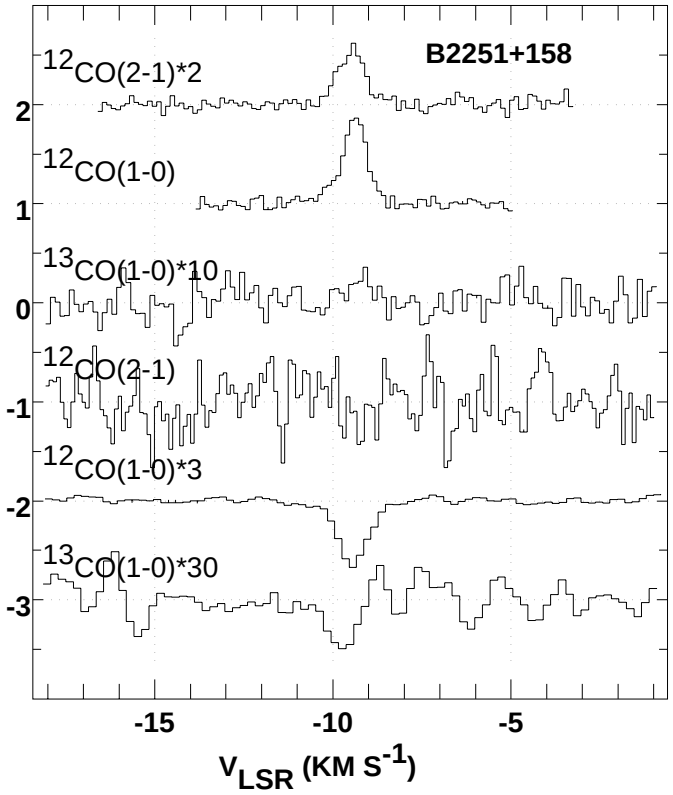

Fig. 10. As in Fig. 1, but for B2251+158 = 3C454.3. The lowest three spectra are in absorption.

order to obtain results free of these effects, we had to use only baselines longer than about 150m (Lucas, 1996).

The CO absorption line survey target list is summarized in Table 1 where we list 1) B1950 source name; 2) any alias; 3)-4) galactic coordinates; 5)-6) the channel-to-channel rms for the line/continuum flux ratio (the rms optical depth noise at zero optical depth) for the ^{12}CO and ^{13}CO J=1-0 line profiles. In Tables 2-3 we present the results of a kinematic decomposition of the line/continuum ratio for the ^{12}CO J=1-0 and J=2-1 profiles; Table 4 shows results for ^{13}CO. The tabulated quantities are obtained from fitting gaussian components of varying optical depth to the absorption (line/continuum) profiles, as is required when the optical depth is not small. For very thick lines, the error estimates for the peak optical should be asymmetrical, and larger on the side of higher optical depth. Those in our Tables simply correspond to the (symmetric) error in the line/continuum ratio, converted to optical depth at the fitted peak value. We were unable to decompose some profiles adequately, notably toward B0212+735 and B0415+379. For the former, Table 2 has an estimate of the integrated optical depth based on a Monte Carlo analysis of the profile, given its rms. This estimate agrees well with a likely gaussian decomposition but for B0415, the J=2-1 line optical depth integral cannot be extracted with any confidence.

2.2. CO emission line profiles

The CO emission line data were taken at the NRAO 12m antenna on Kitt Peak during the period 1992-1997. Results from this telescope are on a scale denoted by $T_{\rm R}^* = T_{\rm A}^*/\eta_{\rm fss}$ where $\eta_{\rm fss}$ is the fraction of the response in the forward direction; $T_{\rm R}^* = \eta T_{\rm mb} \geq 0.7T_{\rm mb}$ for the J=1-0 lines at 110-115GHz and $T_{\rm R}^* \geq 0.5T_{\rm mb}$ for J=2-1. This work used 100 kHz channel spacing and resolution for the earliest spectra, and 48.8 kHz or 97.6 kHz spacing and resolution for the later data. For the ^{12}CO J=1-0 lines, 50 kHz resolution corresponds to 0.13 km s^{-1}.

2.3. Common conventions

All velocities quoted here are measured with respect to the Local Standard of Rest. All limits are twice the empirically-determined rms.

3. Derivations of column density and excitation temperature

The basic equation needed here is the relationship between the column densities N_J in rotation levels J, the optical depths $\tau_{J,J+1}$ of the rotational transitions J→J+1, and the Einstein B-coefficients:

$$\int \tau_{J,J+1} d\nu = (h\nu/c)[N_J B_{J,J+1} - N_{J+1} B_{J+1,J}] \quad (1a)$$

For a linear rotor like CO, this can be recast as

$$N_J = \frac{(2J+1)}{(J+1)} \frac{6.61\times10^{14}{\rm cm}^{-2}\int \tau_{J,J+1}dv}{(\mu/0.11D)^2(1-\exp(-h\nu/kT_{\rm ex}))} \quad (1b)$$

or

$$\frac{N_J}{g_J} = \frac{N_{J+1}}{g_{J+1}} + \frac{6.61\times10^{14}\ {\rm cm}^{-2}}{J+1}\int \tau_{J,J+1}dv \quad (1c)$$

where μ is the permanent dipole moment in Debye (10^{-18} esu; $\mu = 0.11$ D for CO), $\int \tau_{J,J+1}dv$ is in units of km s^{-1}, $T_{\rm ex}$ is the excitation temperature between levels J and J+1, $N_{J+1}/N_J = (g_{J+1}/g_J)\exp(-h\nu/kT_{\rm ex})$, and $g_J = 2J+1$.

By summation from Eqn. 1c we may derive the total column density:

$$N = 6.61\times10^{14}\ {\rm cm}^{-2}\left(\sum_{J=0}^{J=J_a}(J+1)\int\tau_{J,J+1}dv\right) + \frac{(J_a+1)^2}{(2J_a+3)}N_{J_a+1} + \sum_{J=J_a+1}^{J=J_u} N_J$$

where absorption optical depths are measured up to transition $J_a \rightarrow J_a+1$, and J_u is the highest rotational level which is significantly populated. The excitation is usually relatively weak, and most of the CO resides in the lowest two or three levels. The J=3 level of ^{12}CO lies 33 K above the ground state, while typical excitation temperatures are 6 K or less, as we will show.

Table 2. ^{12}CO(J=1-0) absorption line decomposition products[a]

Source	v km s^{-1}	τ_0	FWHM km s^{-1}	$\int \tau dv$ km s^{-1}
B0212	−10.25 (0.05)	0.49 (0.08)	0.73 (0.12)	0.38 (0.09)
	−0.05 (0.03)	0.95 (0.16)	0.45 (0.05)	0.45 (0.09)
	3.5			7.8 (-1,1.2)
B0224	−13.00 (0.17)	0.09 (0.03)	1.12 (0.39)	0.10 (0.05)
	−10.59 (0.03)	0.43 (0.04)	0.84 (0.08)	0.38 (0.05)
	−6.9			0.15 (0.04)
	−4.1			0.10 (0.03)
	−2.75 (0.03)	1.03 (0.07)	0.93 (0.06)	1.02 (0.10)
	−1.24 (0.04)	0.70 (0.05)	1.01 (0.09)	0.76 (0.09)
	0.24 (0.05)	0.23 (0.04)	0.58 (0.12)	0.14 (0.04)
B0355	−18.15 (0.10)	0.17 (0.04)	0.83 (0.09)	0.15 (0.04)
	−17.24 (0.03)	3.13 (0.22)	0.85 (0.02)	2.84 (0.20)
	−13.78 (0.03)	0.26 (0.02)	1.83 (0.08)	0.50 (0.04)
	−13.76 (0.03)	0.22 (0.02)	0.39 (0.04)	0.09 (0.01)
	−10.34 (0.01)	2.00 (0.15)	0.76 (0.01)	1.58 (0.07)
	−8.36 (0.01)	0.86 (0.05)	1.00 (0.02)	0.93 (0.03)
	−4.59 (0.02)	0.60 (0.01)	1.03 (0.04)	0.66 (0.03)
	−3.37 (0.05)	0.18 (0.01)	0.90 (0.10)	0.18 (0.02)
B0528	2.77			<0.11
	9.01 (0.06)	0.23 (0.05)	0.47 (0.14)	0.12 (0.04)
	9.79 (0.02)	2.10 (0.21)	0.52 (0.03)	1.17 (0.14)
B1730	5.08 (0.01)	1.15 (0.06)	0.68 (0.01)	0.83 (0.05)
	6.02 (0.20)	0.08 (0.01)	1.66 (0.31)	0.14 (0.03)
B2013	−55.30 (0.07)	0.39 (0.06)	0.91 (0.15)	0.38 (0.08)
	−39.2			<0.15
	6.63 (0.13)	0.16 (0.03)	2.10 (0.37)	0.36 (0.09)
B2200	−1.43 (0.01)	6.25 (0.80)	0.55 (0.02)	3.67 (0.48)
	−0.76 (0.01)	2.82 (0.14)	1.03 (0.02)	3.08 (0.16)
B2251	−9.43 (0.01)	0.24 (0.01)	0.95 (0.03)	0.24 (0.01)

[a] limits here and in the following tables are 2σ

Table 3. ^{12}CO(J=2-1) absorption line decomposition products

Source	v km s^{-1}	τ_0	FWHM km s^{-1}	$\int \tau dv$ km s^{-1}
B0212	3.2 & 3.8			3.6 (-0.2,2.0)[a]
B0355	−18.51 (0.14)	0.17 (0.08)	0.55 (0.32)	0.10 (0.08)
	−17.18 (0.03)	2.10 (0.29)	0.98 (0.08)	2.21 (0.35)
	−13.91 (0.15)	0.19 (0.06)	1.01 (0.34)	0.20 (0.10)
	−10.18 (0.02)	3.02 (0.57)	0.77 (0.06)	2.48 (0.50)
	−8.39 (0.04)	0.98 (0.12)	0.97 (0.09)	1.01 (0.16)
	−4.76 (0.08)	0.44 (0.07)	1.19 (0.17)	0.55 (0.12)
B0415[a]	-2.8 & -0.9			
B0528	9.77 (0.01)	1.61 (0.11)	0.61 (0.02)	1.05 (0.08)
B1730	5.05 (0.02)	0.69 (0.05)	0.58 (0.03)	0.42 (0.04)
B2200	−1.51 (0.05)	3.38 (1.99)	0.67 (0.09)	2.40 (1.45)
	−0.75 (0.01)	1.83 (0.40)	1.33 (0.17)	2.61 (0.66)

[a] profile too heavily saturated to derive line parameters

Table 4. CO isotope absorption line decomposition products[a]

Source	v km s^{-1}	τ_0	FWHM km s^{-1}	$\int \tau dv$ km s^{-1}
B0212	-10.8			< 0.05[d]
	-0.4			< 0.064
	3.61 (0.03)	0.52 (0.04)	0.89 (0.07)	0.49 (0.06)
B0355	−17.20 (0.03)	0.18 (0.01)	0.91 (0.06)	0.17 (0.02)
	−13.8			< 0.02[d]
	−10.29 (0.03)	0.11 (0.01)	0.61 (0.08)	0.07 (0.01)
	−8.4			< 0.02[d]
	-3.99 (0.12)	0.03 (0.01)	0.76 (0.29)	0.025 (0.01)
B0415	−3.70 (0.02)	0.13 (0.01)	0.41 (0.04)	0.06 (0.01)
	−2.53 (0.01)	1.34 (0.02)	0.89 (0.01)	1.28 (0.03)
	−1.00 (0.01)	0.32 (0.01)	0.98 (0.04)	0.33 (0.02)
B0415[b]	−2.6			0.032 (0.002)
	−0.9			0.014 (0.002)
B0415[c]	−3.68 (0.03)	0.08 (0.01)	0.39 (0.08)	0.03 (0.01)
	−2.56 (0.01)	1.05 (0.02)	0.88 (0.01)	0.99 (0.03)
	−0.89 (0.01)	0.68 (0.02)	0.76 (0.02)	0.55 (0.02)
B0528	9.83 (0.04)	0.038 (0.005)	0.58 (0.09)	0.02 (0.005)
B1730	5.00 (0.06)	0.027 (0.005)	0.68 (0.14)	0.020 (0.004)
	6.3			< 0.014[d]
B2200	−1.31 (0.03)	0.27 (0.02)	1.18 (0.08)	0.34 (0.03)
B2251	−9.6			< 0.01[d]

[a] for ^{13}CO J=1-0 unless otherwise noted
[b] for C^{18}O
[c] for J=2-1
[d] 2σ

3.1. Derivation of excitation temperatures and CO column densities from absorption data alone

Here $J_a = 1$, and

$$N = 6.61 \times 10^{14}\ \mathrm{cm}^{-2} \left(\int \tau_{01} dv + 2 \int \tau_{12} dv \right) + 9/5 N_2$$

So the total column density is directly derived from the measured equivalent widths of the observed transitions, provided we estimate N_2. A lower limit is set by assuming that $T_{\rm ex}$= $T_{\rm cmb}$ for the $J = 1 - 2$ transition; an upper limit is set by assuming that the excitation temperatures for the two lowest transitions are equal. Since N_2 is small, the column density is constrained in a narrow range. Only 10% of the total column density is in the J=2 level when $T_{\rm ex}$(1-0) = 5.5 K.

Column densities (upper and lower limits) derived in this manner for ^{12}CO and ^{13}CO are shown in Tables 5 and 6, respectively, together with the corresponding excitation temperatures of the J=0-1 transition.

3.2. Derivation of excitation temperatures and CO column densities from absorption data and emission data together

Alternatively, the excitation temperature may be derived by comparing the absorption spectrum $(1 - \exp(-\tau))$ with that seen in emission using the relationship

$$T_{\rm R}^{*} = \eta (1 - \exp(-\tau)) * (F(T_{\rm ex}) - F(T_{\rm cmb})) \qquad (2)$$

Table 5. CO column densities and excitation temperatures

Source	v km s^{-1}	N(CO)[a] 10^{15}cm^{-2}	$T_{\rm ex}$(1-0)[a] K	N(CO)[b] 10^{15}cm^{-2}	$T_{\rm ex}$(1-0)[b] K[$\eta=1$]	$T_{\rm ex}$(1-0)[b] K[$\eta=0.7$]	$T_{\rm ex}$(2-1)[b] K[$\eta=1$]	$T_{\rm ex}$(2-1)[b] K[$\eta=0.5$]
B0212	−10.3	<0.73	<3.9	0.50 (0.12)	3.4	3.7		
	0.0	<0.76	<3.8	0.53 (0.10)	<3.1	<3.2		
	3.5			16.0 (2.26)	4.9	6.2	4.8	5.8
B0224	−13.0			0.15 (0.08)	<3.7	<4.1		
	−10.6			0.43 (0.06)	<3.0	<3.1		
	−6.9			0.20 (0.05)	<3.4	<3.8		
	−4.1			0.15 (0.04)	3.7	4.0		
	−2.8			1.59 (0.16)	3.9	4.3		
	−1.2			1.41 (0.17)	4.5	4.9		
	0.2			0.19 (0.05)	3.5	3.8		
B0355	−18.2	0.24	$4.0-4.2$	0.27 (0.07)	4.4	5.8		
	−17.8	$4.9-5.5$	$4.3-4.6$	6.64 (0.47)	5.5	6.6	5.1	6.6
	−13.8	0.67	2.9	1.00 (0.07)	4.2	4.5		
	−10.2	$4.4-7.2$	$6.8-8.5$	4.38 (0.19)	6.4	7.8	5.8	7.6
	−8.4	$2.0-2.5$	$5.3-6.0$	2.60 (0.08)	6.5	8.0	5.2	7.7
	−4	$1.3-1.4$	$4.0-4.1$	1.31 (0.07)	3.9	4.4	3.1	4.0
B0415[c]	−2.5				6.4	7.8	5.7	8.2
	−0.8				8.4	11.4	6.9	9.9
B0528	9.0			0.21 (0.07)	4.2	4.6		
	9.8	$2.2-2.6$	$4.7-5.1$	2.62 (0.31)	5.3	6.6	5.6	7.5
B1730	5.1	1.1	3.5	1.10 (0.07)	3.5	3.7	3.3	3.8
B2013	−55.3			0.85 (0.18)	5.3	6.3		
	6.6			0.44 (0.11)	<3.2	<3.4		
B2200	−1			19.1 (1.59)	6.5	7.9	$\lesssim 6.3$	$\lesssim 9.4$
B2251	−9.4	<1.1	<10.2	0.74 (0.03)	7.0	8.7	6.4	10

[a] from absorption only
[b] from J=1-0 absorption and emission assuming $\eta = 1$
[c] N(CO) $\approx 90 \times 10^{15}$ cm^{-2} from the profile integral in Table 3

where η is a beam efficiency factor for the 12m telescope (nominally > 0.7 for the J=1-0 line and > 0.5 for J=2-1, see Sect. 2) and F(x) = $(h\nu/k)/(\exp(h\nu/kx) - 1)$.

Excitation temperatures derived from the comparison of emission and absorption are also shown in Tables 5 and 6, after those derived from the absorption data alone. Typical rms errors in the excitation temperatures are 0.4-0.6 K at $T_{\rm ex} \approx 5 - 6$ K; they are shown explicitly in Table 6 where results are presented for the isotopic species, including the integrated intensity for the J=1-0 emission profile in ^{13}CO. Given the complexity of some of the observed behaviour, some of the quoted excitation temperatures represent averages over the core regions of the line; in some other cases, upper limits are given, based on 2σ upper limits for $T_{\rm R}^*$.

These excitation temperatures may be compared with those found using the absorption alone, and they may be used to derive the column density in conjunction with the optical depth measurements, which is especially useful in cases where we have measured the absorption in only one line. In the limit of weak excitation, the total ^{12}CO column density is related to the J=1-0 optical depth integral and excitation temperature by $N(^{12}\mathrm{CO})/\int \tau_{J,J+1} dv$ = a(1+b($T_{\rm ex}$(1-0)-$T_{\rm cmb}$)) where a = 1.01×10^{15} cm^{-2}, b = 0.44 for ^{12}CO and a = 1.05×10^{15} cm^{-2}, b = 0.48 for ^{13}CO. These expressions are valid for $T_{\rm ex}$(1-0) $\lesssim$ 6-7 K, in the case of equal excitation temperatures among the lowest few J-levels.

Column densities based on these approximations, with $T_{\rm ex}$ derived from the emission data assuming $\eta = 1$, are shown in Tables 5 and 6 for ^{12}CO and ^{13}CO, respectively. Although we expect (formally) that $\eta < 1$, it is often the case that the excitation temperatures derived from the absorption data alone, which should be well-calibrated, and which rely on two absorption observations of the same gas, fall at the lower end of the range indicated by the absorption-emission comparison.

4. Discussion of derived quantities

4.1. Excitation temperatures and thermal pressure in the ambient gas

Excitation temperatures derived from absorption alone and from the ratio of emission and absorption profiles are shown in Tables 5 and 6. Considering the gross difference between the emission (60″) and absorption beamwidths ($\lesssim 0.001''$) and the inherent calibration errors of the emission results, the table entries seem remarkably consistent. Note that $T_{\rm ex}$(2-1) $\lesssim T_{\rm ex}$(1-0), which justifies the assumption necessary to complete the column density derivation based on the optical depth profiles alone (Sect. 3.1).

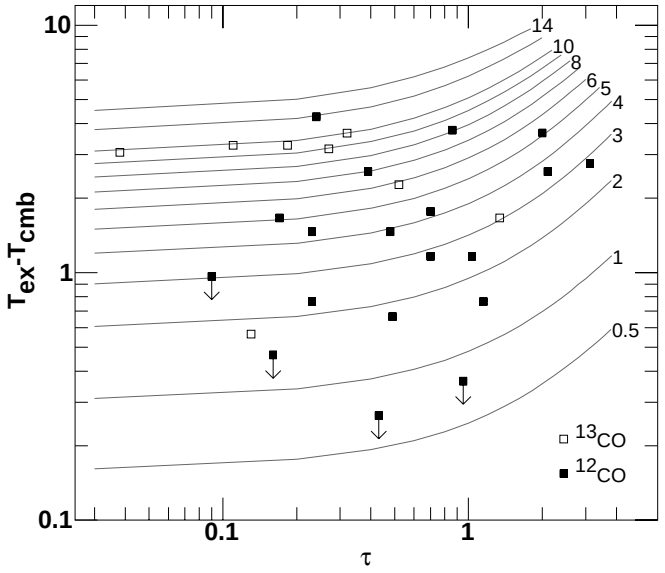

Fig. 11. Derived J=1-0 excitation temperatures plotted against optical depth. In the background are results of an LVG calculation for $T_{\rm K} = 30$K, for various values of the partial pressure of H_2 labelled in units of 10^3 cm^{-3} K. This may be smaller than the actual thermal pressure if there is incomplete conversion of hydrogen to H_2 or if $T_{\rm ex} \approx T_{\rm K}$.

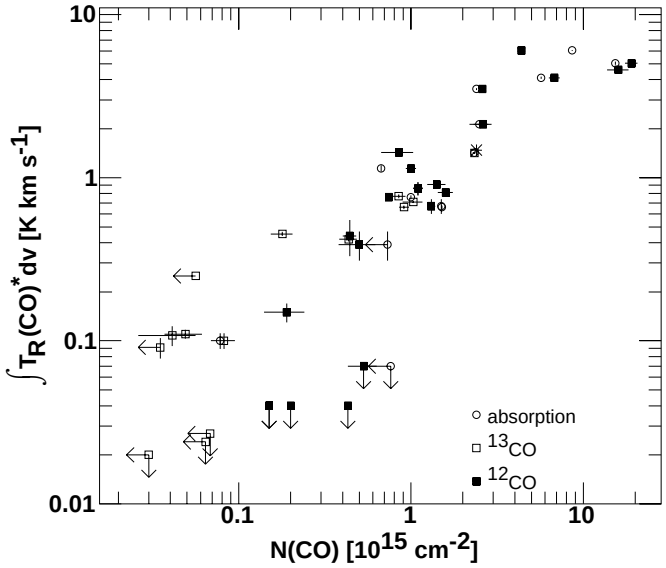

Fig. 12. Variation of carbon monoxide emission line brightness with column density, derived from a comparison of absorption and emission data (solid and open rectangles) and absorption alone (open circles). A point representing observations of the archetypal diffuse cloud toward ζ Oph (Liszt, 1997) is shown as an asterisk at N(CO) = 2.4×10^{15} cm^{-2}.

A comparison of the results in Tables 5 and 6 shows that the excitation temperatures derived from ^{13}CO are typically slightly smaller, which is expected because a lower optical depth provides less radiative excitation during formation of the line. Another way of expressing this would be to say that the apparent optical depth of the ^{13}CO line, derived by assuming that the excitation temperatures of the ^{12}CO and ^{13}CO isotopes are identical, underestimates the true optical depth. In no case have we observed the kind of pumping which may occur in optically thin CO lines when collisions from the J=0 level to J=2, coupled with a relatively rapid J=2-1 decay, overpopulate the J=1 level (Leung and Liszt, 1976). Obviously we also see no sign of population inversion (negative excitation temperatures).

^{12}CO and ^{13}CO J=1-0 excitation temperatures are plotted against optical depth in Fig. 11, superimposed against the predictions of an LVG model (Goldreich and Kwan 1974, but using modern cross-sections and accounting for He) at an assumed temperature $T_{\rm K} = 30$K. In the limit that $T_{\rm ex} << T_{\rm K}$, $T_{\rm ex}$ depends on the product $p = n(H_2) * T_{\rm K}$, rather than on $n(H_2)$ or $T_{\rm K}$ alone. The median partial pressure of H_2 for all ^{12}CO features is $n(H_2)T_{\rm K} = 3.2 \times 10^3$ cm^{-3} K. For most of the lines of sight studied here, the pressure estimates are valid even if $T_{\rm K}$ is as low as 10 K.

Clearly, the ^{13}CO lines for which we were able to determine an excitation temperature (Fig. 11) arise preferentially in higher-pressure clouds. This may result from an obvious selection bias toward stronger features. But the slightly lower $T_{\rm ex}$ found for ^{13}CO, compared to ^{12}CO in the same features, show that ^{13}CO is not sequestered in high-pressure regions within individual clouds (see Tables 5 and 6). There is also no tendency for $T_{\rm ex}$ to increase with τ or N(CO) for the majority of features studied in ^{12}CO, at least at $\tau \leq 1$. The pressures found from this analysis overlap entirely with those derived by Jenkins et al. (1983) from $Copernicus$ spectra of neutral carbon in classical diffuse clouds and are often quite small compared to those of even a modest dark cloud ($T_{\rm K} = 12$ K, $n(H_2) = 1000$ cm^{-3}).

4.2. CO column density and emission line brightness

Column densities for ^{12}CO are presented in Table 5, derived from the absorption alone, where possible, and for the combination of emission and absorption data. The differences between the two sets of numbers, which are seldom large, can be traced to obvious differences in the inferred excitation. The CO column densities are of necessity extremely modest because the excitation temperatures are low and the line profiles are not saturated beyond recognition ($i.e.$ decomposition).

The variation of CO emission intensity with column density is shown in Fig. 12; points representing both derivations of the latter are shown. With care, emission may occasionally be detected from absorption features corresponding to $N(^{12}$CO) as small as 2×10^{14} cm^{-2} or $N(^{13}$CO) $= 4 \times 10^{13}$ cm^{-2}, but several features with similarly low $N(^{12}$CO) were not detected at even lower limits. Molecular emission is not secure until $N(^{12}$CO) $\approx 5 \times 10^{14}$ cm^{-2}.

It is important to note that, when N(CO) is derived from a comparison of absorption and emission using the approximations discussed in Sect. 3.2, N(CO) $\propto T_{\rm ex} \int \tau dv$ for $T_{\rm ex} > 5$K, and $T_{\rm ex} \propto T_{\rm R}^*/\tau$ for small optical depth. So N(CO) $\propto \int T_{\rm R}^* dv$ in some cases and a strong seeming correlation between brightness and column density can easily be created. However the optical

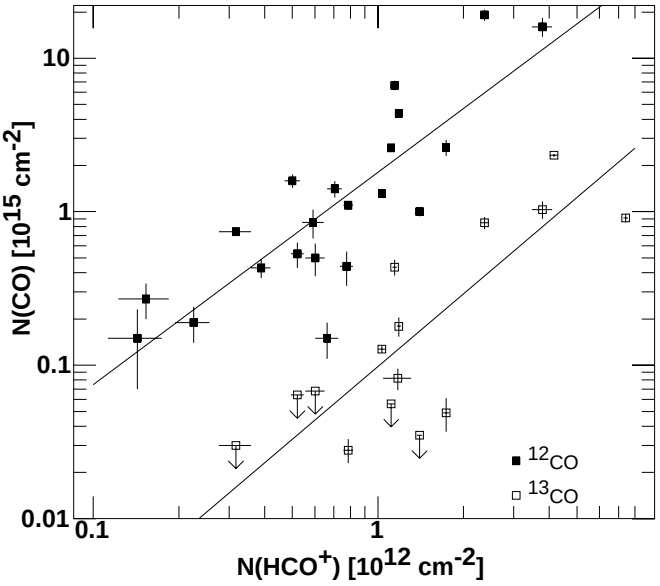

Fig. 13. Variation of ^{12}CO and ^{13}CO column density with HCO$^+$. The power-law slopes of the regression lines shown are 1.4 for ^{12}CO and 1.6 for ^{13}CO.

depth of most of the ^{12}CO lines is not small and we have a means of deriving N(CO) without recourse to the absorption-emission comparison in many cases. The behaviour in Fig. 12 is not an artifact even for those cases in which the emission profiles were used to derive $T_{\rm ex}$ and N(CO).

The variation of the derived ^{12}CO and ^{13}CO column densities is shown in Fig. 13, plotted $vs.$ the column density of HCO$^+$ which we discussed in LL96. In both cases, the CO abundance increases abruptly at N(HCO$^+$) $\approx$ 10^{12} cm^{-2} which is familiar behaviour from our prior work on other species such as HCN (Lucas and Liszt, 1996, 1997); by contrast, HCO$^+$ and OH show a strict linear proportionality over the same regime (Liszt and Lucas, 1996). CO becomes self-shielding against photodissociation by the interstellar radiation field at N(CO) $\gtrsim$ 10^{14} cm^{-2} (Bally and Langer, 1982; Van Dishoeck and Black, 1988) and its abundance relative to H_2 is expected to increase by several orders of magnitude over a fairly limited range of visual extinction (Kopp et al., 1996).

4.3. CO isotopic abundances

Column densities of ^{13}CO or C^{18}O can be derived in the same manner as for ^{12}CO and isotopic column density ratios are summarized in Table 7 and Fig. 14. Those clouds having the highest CO column densities typically show ^{13}CO enhancements of 3 to 4 relative to ^{12}CO with ^{12}CO/^{13}CO= 15-20 compared to an expected intrinsic ratio ^{12}C/^{13}C = 60 in the gas at large (Lucas and Liszt, 1998). Clouds with lower N(CO) have higher carbon isotope ratios, with ^{13}C enhanced by at most a factor of two. This trend is expected because there is in principle little that can be done by either selective photodissociation or fractionation at very small CO column densities to make the isotope ratios in CO differ from those in the ambient gas. When N(CO) is very small, none of the isotopes are self-shielding and the photodissociation rate is equally large for all (barring accidental line overlaps with transitions of H_2). When the photodissociation rate is high, individual CO molecules are formed and destroyed before the ^{13}C-fractionation reaction can establish equilibrium.

We were not able to measure both the ^{12}CO/^{13}CO and ^{13}CO/C^{18}O ratios in absorption in the same direction but the ^{13}CO/C^{18}O ratios observed in absorption and emission toward 3C111 agree quite well. Our data do not require a deficit of C^{18}O except in the -10 km s^{-1} cloud toward B0355[2]. The expected intrinsic value of the carbon/oxygen double isotope ratio in the gas is $\approx$ 9, with ^{12}C/^{13}C = 60 (Lucas and Liszt, 1998) and ^{16}O/^{18}O = 560 (Wilson and Rood, 1994).

The degree of ^{13}CO enhancement we find is somewhat greater than predicted. Models of the envelopes of translucent clouds show that fractionation generally prevails over selective photodissociation of ^{13}CO and is particularly effective at $A_{\rm V} \approx 0.5$ mag where ^{13}CO/^{12}CO is enhanced very locally by factors of 5 to 20 at 50 and 15 K, respectively (see Fig. 12 of Van Dishoeck and Black 1988, noting that their work assumed [^{12}C/^{13}C] = 45). But this occurs at relatively low CO abundances and none of the models show enhancements of ^{13}CO by more than a factor of two when integrated over an entire sightline having an appreciable CO column density, $i.e.$ through a gas column as large as $A_{\rm V} \approx 1$. Models of the gas around ζ Oph by Kopp et al. (1996) show similar underestimation of the degree of ^{13}CO fractionation seen here, with $N(^{12}{\rm CO})/N(^{13}{\rm CO})$ observed to be 20 in emission, while the models predict values of 30. The models seem to require an enhanced radiation field and relatively high number density (typically 3000 H_2 cm^{-3}) to provide substantial enhancement of ^{13}CO. Neither of these conditions seems applicable to the clouds observed here.

Our data show unambiguously that fractionation effects (Watson et al., 1976) are important at CO column densities as low as 1-4 $\times$ 10^{15} cm^{-2} and that the fractionation of ^{13}CO dominates over its selective photodissociation even at the extremely low CO column densities encountered here. The ^{13}CO/C^{18}O ratio remains high even in very diffuse gas. Rather different conclusions have been reached from studies of CO emission at the periphery of dark clouds by Langer et al. (1989, LWGB) and Lada et al. (1994) but our data are in fact consistent with their earlier observational results as we show in Sect. 5.

Because the relative abundance of ^{13}CO is so strongly enhanced, the ^{12}CO optical depth is much smaller than would be estimated from a simple scaling of the ^{13}CO line using a Solar or typical interstellar carbon isotope ratio. In fact this very situation caused some interpretative difficulties for Kobulnicky et al. (1995) who studied molecular absorption along the line of sight to B2023+336 (see also Liszt and Lucas, 1996). By chance, fractionation is quite strong in this direction, where the ratio of peak emission strengths in ^{12}CO and ^{13}CO is 14:1 even when $\tau(^{12}{\rm CO}) \approx 0.5$. Their speculation about source covering and beam-filling factors is probably unwarranted.

[2] for C^{18}O this limit required nearly nine hours of integration

Table 6. ^{13}CO column density, J=1-0 excitation temperature, and emission brightness

Source	v km s^{-1}	$N(^{13}\mathrm{CO})^a$ 10^{14} cm^{-2}	$T_{\rm ex}{}^a$ K	$N(^{13}\mathrm{CO})^b$ 10^{14} cm^{-2}	$T_{\rm ex}{}^b$ K[$\eta = 1$]	$T_{\rm ex}{}^b$ K[$\eta = 0.7$]	$\int T_{\rm R}^* dv$ K km s^{-1}
B0212	-10.2			$<$0.68	3.4^c		< 0.027
	-0.4			< 0.64	3.1^c		< 0.029
	3.6			10.3 (1.36)	5.0 (0.5)	5.7 (0.6)	0.71
B0355	-17.2			4.34 (0.51)	6.0 (0.9)	7.2 (1.2)	0.51
	-13.8			$<$0.35	4.2^c		0.09
	-10.3			1.79 (0.26)	6.0 (0.7)	7.2 (1.0)	0.45
	-8.4			$<$0.56	6.5^c		0.25
	-4.0			0.41 (0.16)	3.9^c		0.11
B0415	-3.7	$0.81 - 0.83$	$3.45 - 3.55$	0.82 (0.13)	3.5^c		0.10
	-2.6	$22.1 - 24.5$	$4.4 - 4.6$	23.3 (0.50)	4.4 (0.4)	5.7 (0.6)	1.42
	-0.8	$9.8 - 16.6$	$7.1 - 9.2$	9.1 (0.60)	6.4 (0.6)	7.9 (0.6)	0.66
B0528	9.8			0.49 (0.12)	5.8 (0.5)	6.9 (0.7)	0.11
B1730	5.0			0.28 (0.05)	3.5^c		
B2200	-1.3			8.48 (0.78)	5.9 (0.7)	7.1 (0.9)	0.77
B2251	-9.6			< 0.30	7.0^c		< 0.02

^{a} from absorption only
^{b} from absorption and emission
^{c} assumed; from ^{12}CO

4.4. Linewidths

The widths of the observed CO lines are presented in the form of FWHM for gaussian fits to the absorption line profiles in Tables 2-4; they have not been corrected for the instrumental resolution of 140 kHz (0.36 km s^{-1} for ^{12}CO). The mean tabulated linewidth is 0.84 ± 0.31km s^{-1}, which becomes 0.76 ± 0.28 km s^{-1} after subtracting the channel width in quadrature. There is too little overlap between the sets of well-measured ^{12}CO and ^{13}CO profiles to compare their widths in detail, although the few points plotted for ^{13}CO in Fig. 10 have typical values.

The ^{12}CO J=1-0 linewidths are slightly but noticeably narrower than those found for HCO$^+$. The mean deconvolved FWHM for the two species, for those features shown in Fig. 15, are 0.75 ± 0.28 km s^{-1}and 0.86 ± 0.29 km s^{-1}. This result is suggestive but may suffer somewhat from the relatively low resolution used here. The channel width is 30% higher at the HCO$^+$ line.

Table 7. CO isotope ratios

Source	v km s^{-1}	^{12}CO/^{13}CO	^{13}CO/C^{18}O ^{a}	^{13}CO/C^{18}O ^{b}
B0212	3.6	15.5 (3.0)		25 (3)
B0355	-17.8	15.3 (2.1)		> 36.0
	-13.8	> 28.6		
	-10.2	24.5 (3.7)		> 53.6
	-8.4	> 46.4		
	-4.0	32.3 (13.1)		> 24.7
B0415	-2.6		40 (2.7)	25.6 (2.3)
	-0.8		23.6 (3.7)	25.8 (6.0)
B0528	9.7	53.5 (13)		
B1730	5.2	39.3 (7.4)		
B2200	-1	22.5 (2.8)		
B2251	-9.6	> 24.7		

^{a} ratio of J=1-0 optical depths
^{b} ratio of $\int T_{\rm R}^*(1-0)dv$

4.5. Comparison of emission and absorption profiles

There are some remarkable coincidences between the emission and absorption profiles, perhaps best exemplified in the zero-velocity gas toward B0224+671. The ratio of these two profiles, which is essentially the excitation temperature averaged over the gas column at each velocity, is clearly a constant such that the gas has a uniform excitation in the line core and wings. There is in general no tendency for the excitation temperatures derived in this way either to peak at the line center (which might reflect the effects of radiative trapping) or in the wings (which, mimicking H I, would indicate a blending of material with disparate excitation temperatures). In H I, the derived spin temperature decreases at the centers of absorption features (Dickey et al., 1979) because the emission profile is a blend of cooler and warmer gases. The cooler gas absorbs more strongly on a per-atom basis and the excitation and kinetic temperatures are tightly coupled. For weakly excited CO, the excitation temperature is determined largely by the thermal pressure (see Sect. 4.1) so that a cloud made up of clump and interclump material in thermal pressure equilibrium would show no such effect.

As we have noted before, and unlike H I, (Dickey et al., 1979; Clark, 1965), the absorption lines of HCO$^+$ and CO are, if anything, wider and more common than their emission counterparts. However, we believe we have now seen one candidate where an emission line may not have an absorption counterpart. The weak, redshifted wing on the J=1-0 ^{12}CO and ^{13}CO emission profiles toward B0528+134 is not matched in absorption. This could be a lump in the

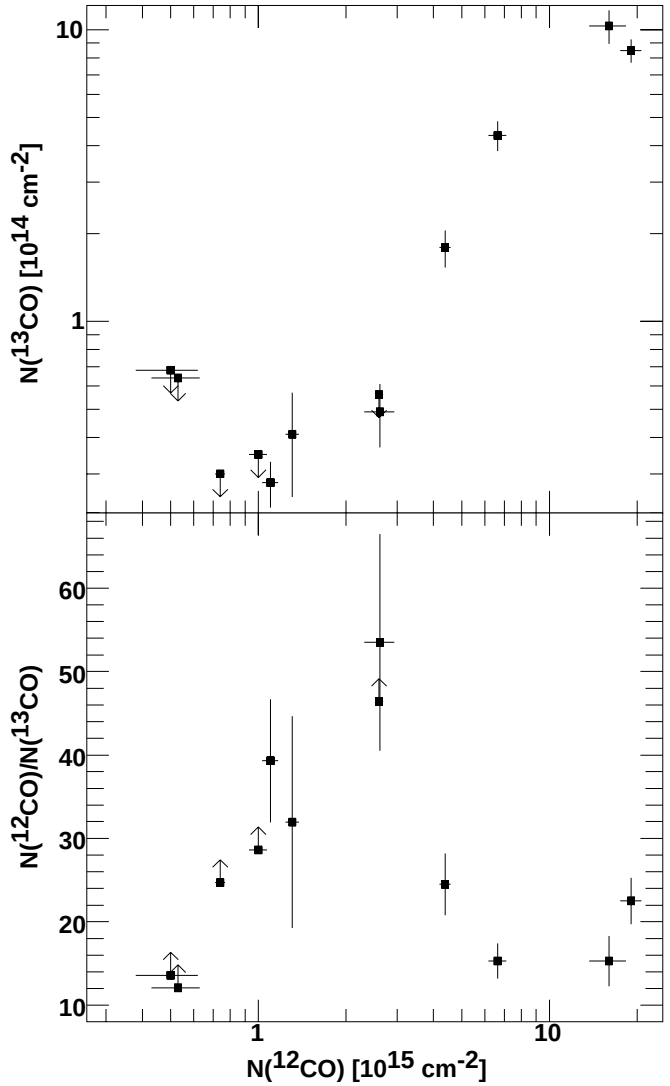

Fig. 14. Variation of ^{13}CO column density (top) and ^{13}CO/^{13}CO isotopic abundance ratio with $N(^{12}\mathrm{CO})$.

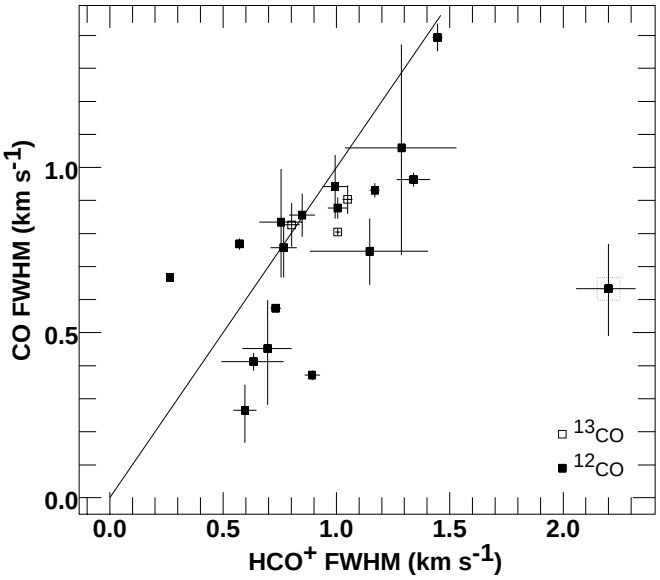

Fig. 15. CO J=1-0 linewidths $vs.$ those found previously for HCO^+ by Lucas and Liszt (1996). The linewidths have been corrected for the instrumental resolution of 140 kHz. One outlying point, the -11 km s^{-1} feature toward B0212+735, is marked. For the strong features toward B0212+735 and 3C111, data are plotted for ^{13}CO. The mean CO FWHM linewidth is 87% that of HCO^+ (0.75 $vs.$ 0.86 km s^{-1}). The line shown is for equal widths.

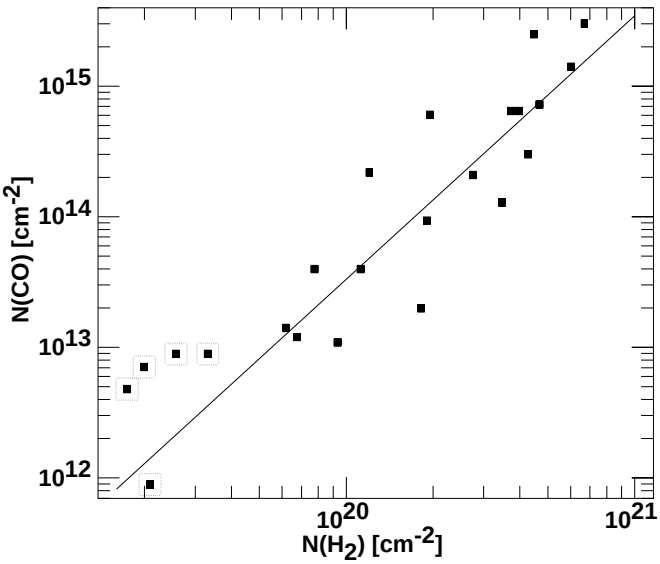

Fig. 16. CO and H_2 column densities determined in the UV, taken from the 1995 revision of the compilation of Federman et al. (1994). The power-law slope of the regression line shown is 2.02 ± 0.29. Some outlined points at very low $N(H_2)$ were not used in calculating this line.

gas which does not occult the continuum or a low column density component with a high excitation temperature. Another interesting case occurs at -9 km s^{-1} toward B0355+508 because the adjacent features are much more clearly separated in absorption than in emission.

5. Discussion

5.1. Physical conditions and chemical abundances of CO, OH, and HCO$^+$

Local CO can now be detected over an enormous range of column density at mm-wavelengths. The weakest ^{12}CO absorption lines found here, with N(CO) of order 10^{14} cm^{-2}, have column densities which are more than 10^5 times lower than those seen in emission toward dense cores in local dark clouds like ρ Oph or local GMC's like Orion KL. Conversely, features with N(CO) as large as even 2×10^{16} cm^{-2}, containing only ten percent of the carbon nuclei in a gas column having $A_V = 1$ mag, are already so optically thick in the lines of ^{12}CO that they can only barely be analyzed.

We argue that the clouds we have observed are classically diffuse or marginally translucent, from the following evidence; the small values of N(CO) compared to the amount of total amount of gas-phase carbon expected for $N(H_2)$ =

4×10^{20} cm^{-2} [3]; the moderate, median, partial thermal pressure $n(H_2)T_K = 3.2 \times 10^3$ cm^{-3} K; and the high degree of ^{13}CO fractionation commonly observed. Thus the gas is cool and most of the carbon is in C^+. The latter inference can be tested because the column density of neutral carbon could be quite high, of order 10^{17} cm^{-2} in many cases. We have reached similar conclusions before without such detailed knowledge of the CO, on the basis of comparisons of CO emission with OH and HCO^+ absorption (LL96).

The variation of N(CO) with $N(H_2)$ as determined from optical absorption-line measurements is summarized by Federman et al. (1994) and shown in Fig. 16. As noted in LL96, the occurrence of CO with N(^{12}CO) $\gtrsim 10^{15}$ cm^{-2} coincides with the increase of the N(CO)/$N(HCO^+)$ ratio at $N(HCO^+)$ = $1 - 2 \times 10^{12}$ cm^{-2}, N(OH) = 4×10^{13} cm^{-2}. It has been our surmise that HCO^+, along with OH, shows a near-constant abundance relative to H_2. In the optical data $N(CO) \propto N(H_2)^{2.0}$ while N(CO) varies at least as rapidly as $N(CO) \propto N(HCO^+)^{1.5}$ (Fig. 13). The abundances of CO and HCO^+ (but not, apparently, OH) are a substantial embarrassment to conventional models of gas-phase chemistry in low-density, moderate-extinction regions (see Liszt and Lucas, 1994, and LL96). But, if CO forms from HCO^+, solution of the HCO^+ problem solves the CO problem as well.

5.2. Persistence of isotope-altering effects at low N(CO) and A_V

Perhaps the most striking result of this work is the strong fractionation of ^{13}CO (Watson et al., 1976) for N(^{12}CO) $\gtrsim 10^{15}$ cm^{-2}. Models of diffuse regions show little fractionation because the photoionization rate is too large and the abundance of CO is too small. Models of translucent clouds, which try to reproduce the observable properties of denser and darker gas than we believe are relevant here, show important fractionation effects over only limited regions and produce overall enhancements of ^{13}CO which are somewhat smaller than those seen here (see Van Dishoeck and Black, 1988; Kopp et al., 1996).

Model results aside, the common enhancement of ^{13}CO and high ^{13}CO/C^{18}O ratios were for some time quite puzzling to us, because our understanding was based largely on the results of two comprehensive studies of the behaviour of CO emission at the edges of dark clouds by LWGB and Lada et al. (1994). These papers, where maps of J=1-0 emission from the three most common CO isotopes were compared with star counts and dust emission as tracers of the extinction, deprecate the importance of any isotope-selective effects at extinctions $A_V \lesssim 5$ mag. They used similar molecular emission data and methodologies so we will discuss only the earlier of them in detail.

[3] At such N(H_2) CO begins to appear in emission at the 1 K level with $N(CO) \approx 10^{15}$ cm^{-2}, and H_2 typically contains half of the H-nuclei along an entire line of sight, see Savage et al. 1977, Fig. 8 of LL96, and Fig. 12 here

LWGB in their discussion (their Sect. IV b and Fig. 5 at top), claim to show that the ^{13}CO/C^{18}O emission intensity ratio peaks for moderate extinctions at values 20 ± 10 and declines precipitously, to the Solar value of 5.5, for $A_V < 2$ mag, $N(^{13}CO) < 4 \times 10^{15}$ cm^{-2}, $\int T_R^*(^{13}CO)dv < 4$ K km s^{-1}. Clearly our ^{13}CO column densities and integrated intensities are so small (Table 6) that no alteration of either the ^{12}CO/^{13}CO or ^{13}CO/C^{18}O ratios would be expected if this assertion were correct.

LWGB drew their conclusions from a plot of the ^{13}CO/C^{18}O integrated intensity ratio $vs.$ ^{13}CO line integral, displaying data only for those positions at which the rarer isotope was detected (their Fig. 5 at top). From their Fig. 5 at bottom, it is easy to see that this detection threshold was 0.12 K km s^{-1} (in the text they quote 0.1 K km s^{-1}). Thus, for any given ^{13}CO line integral the ^{13}CO/C^{18}O integrated intensity ratio has an upper bound $\int T_R^*(^{13}CO)dv / \int T_R^*(C^{18}O)dv \leq \int T_R^*(^{13}CO)dv/0.12$ K. This coincides exactly with the upper envelope of the plotted data over that range for which the decline in ^{13}CO/C^{18}O is claimed. Put another way, their C^{18}O observations were simply not sensitive enough to detect C^{18}O reliably for ^{13}CO line profile integrals below 4 K km s^{-1}, precisely because the ^{13}CO/C^{18}O ratio is often so large (25-40) at low extinction and column density.

That the claimed decline is an artifact of this effect can be seen clearly in Fig. 5 of LWGB at bottom, where the isotope ratio is plotted against the $\int T_R^*(C^{18}O)dv$ profile integral. Both the mean isotopic intensity ratio and its scatter increase steadily down to the detection limit of the C^{18}O at 0.12 K km s^{-1} with no suggestion of a turnover. Lada et al. (1994) claim that the ^{13}CO/C^{18}O ratio peaks at a value 16$\pm$10 for $A_V = 5$ mag, declining to the solar system ratio of 5.5 at low or high extinction. They only show their data in binned format but comment on the high dispersion of the mean isotope ratio at lower $N(^{13}CO)$ and suggest that it is "unstable" at low extinction; this effect is probably an artifact of low signal/noise as well. In any case, the ^{12}CO/^{13}CO ratio expected for the local interstellar medium clearly lies in the range 8 - 10, because ^{12}C/^{13}C = 60, not 89, and ^{16}O/^{18}O$\gtrsim$ 560 (Wilson and Rood, 1994; Lucas and Liszt, 1998).

The strong ^{13}CO enhancement in our data is in disagreement with the carbon isotope ratio found from HST spectra by Lambert et al. (1994) toward ζ Oph, where N(^{12}CO) = 2.4×10^{15} cm^{-2} and ^{12}CO/^{13}CO = 167 (but see Lyu et al., 1994). Carbon isotope ratios seen in mm-wave emission toward ζ Oph are in the range 60-80 with substantial errors (Langer et al., 1987; Wilson et al., 1992), while only 10′–20′ away (0.5-1.0 pc) the ratio drops to values of 25-45 as N(CO) increases under the influence of its own self-shielding within a more or less fixed hydrogen column density (Liszt, 1997; Kopp et al., 1996).

5.3. The dimensionality of diffuse gas

The molecular gas is surprisingly one-dimensional; integration along the line of sight to a point source whose size is known

from VLBI to be $< 0.001''$ is sufficient to produce a fully-formed line profile which bears an uncanny resemblance to that seen in emission on arcminute scales. Although this similarity would arise trivially in a uniform medium, or in a slab geometry where all structure is thin along the line of sight and broad across it, these trivial cases will not produce spatial structure in the molecular emission. Yet molecular emission is structured, perhaps quite heavily so (Falgarone and Phillips, 1996), and the gas toward our sources shows clear structure in emission as well (Liszt and Wilson, 1993). Detailed models of this gas must meet seemingly contradictory requirements, not allowing averaging over the emission beam to destroy the essential similarity of the emission and absorption profiles, but still producing emission maps which are not entirely featureless. It would be interesting to be able to compare the absorption and emission profiles from modern turbulent cloud models such as those discussed by Falgarone et al. (1994) and Falgarone et al. (1995).

6. Summary

Using the IRAM Plateau de Bure Interferometer and the NRAO 12m telescope, we have observed mm-wave carbon monoxide absorption and emission in the regime where it first becomes detectable, at column densities $N(^{12}\mathrm{CO}) \geq 10^{14}$ cm^{-2} typically seen in uv absorption against nearby bright stars. HCO^+ and OH absorption features have CO absorption counterparts but CO emission does not become prominent until $N(\mathrm{CO}) \geq 5 \times 10^{14}$ cm^{-2}. This reflects the fact that molecules like OH, HCO^+, and CO form in low- pressure diffuse environments as soon as the fraction of H_2 is appreciable, at $N(\mathrm{H}) \geq 4 \times 10^{20}$ cm^{-2}, but even CO cannot be appreciably rotationally excited at the very lowest thermal pressures which are encountered. From measurements of the CO optical depth and excitation temperature we find a median thermal pressure $n(\mathrm{H_2})T_\mathrm{K} = 3.2 \times 10^3$ cm^{-3} K with values distributed over the range $n(\mathrm{H_2})T_\mathrm{K} = 0.5 - 12 \times 10^3$ cm^{-3} K.

Thus, the clouds we have studied range from classically diffuse ($A_\mathrm{V} << 1$) to barely translucent ($A_\mathrm{V} \gtrsim 1$). Over this regime, uv absorption studies have shown that $N(\mathrm{CO}) \propto N(\mathrm{H_2})^2$, with perhaps a somewhat sharper turn-on at $N(\mathrm{H_2}) \approx 4 \times 10^{20}$ cm^{-2}, $N(\mathrm{CO}) \approx 10^{15}$ cm^{-2}. In analogous fashion, we find that $N(\mathrm{CO}) \propto N(\mathrm{HCO^+})^\alpha, \alpha \approx 1.5$, with perhaps a sharper turn-on at $N(\mathrm{HCO^+}) \approx 10^{12}$ cm^{-2}, $N(\mathrm{CO}) \approx 10^{15}$ cm^{-2}. Lines of HCO^+ are slightly broader than those of CO, with mean FWHM of 0.86 and 0.75 km s^{-1}, respectively.

By the time A_V approaches unity along some lines of sight, the ^{12}CO lines are so optically thick that they cannot be easily analyzed. Lines of ^{13}CO are optically thin in most cases, but the ^{13}CO/^{12}CO abundance ratio is often surprisingly large. We find that $N(^{13}\mathrm{CO})$ is usually enhanced through chemical fractionation (insertion of ^{13}C *via* $^{13}C^+$), by factors as large as 3-4 relative to the local interstellar carbon isotopic abundance ratio [^{12}C]/[^{13}C] = 60. ^{12}CO optical depths are generally much smaller than would be inferred by the simple scaling $\tau(^{12}\mathrm{CO}) = 60\tau(^{13}\mathrm{CO})$. We see no evidence for any diminution of the ^{13}CO/^{12}CO ratio which could result from selective photodissociation effects, as apparently occurs in the gas around ζ Oph.

Although we detect ^{13}CO more easily in higher column density, higher-pressure environments, the excitation temperatures derived for ^{13}CO are slightly below those of ^{12}CO, consistent with a smaller degree of resonant excitation. From this, we infer that ^{13}CO is not sequestered in limited, higher-pressure regions of the CO-bearing gas. The $C^{18}O$ isotope is quite difficult to detect in all of our features, with $N(^{13}\mathrm{CO})/N(\mathrm{C^{18}O})$ ratios typically 25-40 as compared to the local interstellar value of 8. Most of the difference can also be explained by enhancements to $N(^{13}\mathrm{CO})$, with little selective photodestruction even of $C^{18}O$. The persistence of ^{13}CO-enhancements at small A_V contradicts the conclusions of two recent comprehensive studies of extinction and CO emission at the edges of dark clouds. We showed that the contradiction arises from a rather obvious error of interpretation in the earlier work.

Comparison of CO absorption and emission profiles shows that the same gas is sampled over a very wide range of beam-sizes ($i.e.$ $< 0.001''$ in absorption and $60''$ in emission). The linewidths are generally the same and the excitation temperatures derived from a comparison of emission and absorption are the same as those derived from absorption alone. Although it would be easy to manufacture these similarities in uniform clouds, the presence of small-scale spatial structure, which is always seen in emission, might have been expected to induce substantial distortions into the more macroscopic emission beams. The emission-absorption comparison also shows that there are no clear lines of sight through the gas. Should such gaps exist we would expect absorption against the compact mm-wave sources to be less common, or to have less fully-developed line profiles compared to the emission. Neither is the case.

Acknowledgements. The National Radio Astronomy Observatory (NRAO) is operated by Associated Universities, Inc. (AUI) under a cooperative agreement with the US National Science Foundation.

References

Langer, W. D., Glassgold, A. E., and Wilson, R. W.: 1987, ApJ 322, 450
Bally, J. and Langer, W. D.: 1982, ApJ 255, 143
Clark, B. G.: 1965, ApJ 142, 1398
Dickey, J. M., Terzian, Y., and Salpeter, E. E.: 1979, ApJ 228, 465
DuPuy, D., Schmitt, J., McClure, R., Van Den Bergh, S., and Racine, R. P.: 1969, ApJ 156, L135
Falgarone, E., Lis, D. C., Phillips, T. G., Pouquet, A., Porter, D. H., and Woodward, P. R.: 1994, ApJ 436, 728
Falgarone, E. and Phillips, T. G.: 1996, ApJ 472, 191
Falgarone, E., Pineau Des Forets, G., and Roueff, E.: 1995, A&A 300, 870
Federman, S. R., Strom, C. J., Lambert, D. L., Cardelli, J. A., Smith, V. V., and Joseph, C. L.: 1994, ApJ 424, 772
Goldreich, P. and Kwan, J.: 1974, ApJ 189, 441
Guilloteau, S., Delannoy, J., Downes, D., Greve, A., Guelin, M., Lucas, R., Morris, D., Radford, S. J. E., Wink, J., Cernicharo, J., Forveille, T., Garcia-Burillo, S., Neri, R., Blondel, J., Perrigourad, A., Plathner, D., and Torres, M.: 1992, A&A 262, 624

Hogerheijde, M. R., De Geus, E. J., Spaans, M., Van Langevelde, H. J., and Van Dishoeck, E. F.: 1995, ApJ 441, L93
Jenkins, E. B., Jura, M., and Loewenstein, M.: 1983, ApJ 270, 88
Kobulnicky, H. A., Dickey, J. M., and Akeson, R. L.: 1995, ApJ 443, L45
Kopp, M., Gerin, M., Roueff, E., and Le Bourlot, J.: 1996, A&A 305, 558
Lada, C. J., Lada, E. A., Clemens, D. P., and Bally, J.: 1994, ApJ 429, 694
Lambert, D. L., Sheffer, Y., Gilliland, R. L., and Federman, S. R.: 1994, ApJ 420, 756
Langer, W. D., Wilson, R. W., Goldsmith, P. F., and Beichman, C. A.: 1989, ApJ 337, 355, (LWGB)
Leung, C. M. and Liszt, H. S.: 1976, ApJ 208, 732
Liszt, H. S.: 1994, ApJ 429, 638
Liszt, H. S.: 1997, A&A 322, 962
Liszt, H. S. and Lucas, R.: 1994, ApJ 431, L131
Liszt, H. S. and Lucas, R.: 1996, A&A 314, 917
Liszt, H. S. and Wilson, R. W.: 1993, ApJ 403, 663
Lucas, R.: 1996, in P. A. Shaver (ed.), *Science with Large Millimetre Arrays, (ESO-IRAM-NFRA-Onsala Workshop, held at Garching, Germany, 11-13 December 1995), Springer-Verlag Berlin Heidelberg New York.*, pp 185–192
Lucas, R. and Liszt, H. S.: 1993, A&A 276, L33, (LL93)
Lucas, R. and Liszt, H. S.: 1994, A&A 282, L5, (LL94)
Lucas, R. and Liszt, H. S.: 1996, A&A 307, 237, (LL96)
Lucas, R. and Liszt, H. S.: 1997, in D. J. Jansen, M. R. Hogerheijde, and E. F. Van Dishoeck (eds.), *Molecules in astrophysics: Probes and processes (IAU Symposium 178, held in Leiden, The Netherlands, July 1-5, 1996), Leiden: Kluwer*, p. 421, (LL97)
Lucas, R. and Liszt, H. S.: 1998, A&A, in press (LL98)
Lyu, C.-H., Smith, A. M., and Bruhweiler, F. C.: 1994, ApJ 426, 254
Marscher, A. P., Bania, T. M., and Wang, Z.: 1991, ApJ 371, L77
Morton, D. C.: 1975, ApJ 197, 85
Savage, B. D., Drake, J. F., Budich, W., and Bohlin, R. C.: 1977, ApJ 216, 291
Ungerer, V., Nguyen-Quang-Rieu, Mauron, N., and Brillet, J.: 1985, A&A 146, 123
Van Dishoeck, E. F. and Black, J. H.: 1988, ApJ 334, 771
Watson, W. D., Anicich, V. G., and Huntress, W. T., J.: 1976, ApJ 205, L165
White, G. J.: 1997, in W. B. Latter, S. J. E. Radford, P. R. Jewell, J. G. Mangum, and J. Bally (eds.), *CO: twenty-five years of millimeter-wave spectroscopy (IAU Symposium 170, held in Tucson, Arizona, May 29 - June 5, 1995), Dordrecht: Kluwer, 1997*, pp 101–109
Wilson, T. L., Mauersberger, R., Langer, W. D., Glassgold, A. E., and Wilson, R. W.: 1992, A&A 262, 248
Wilson, T. L. and Rood, R.: 1994, ARA&A 32, 191